

First measurements from charmless B decays at Belle II

Yun-Tsung Lai^{*†}

Kavli IPMU

E-mail: yun-tsung.lai@ipmu.jp

We report on first measurements of branching fractions and CP -violating charge-asymmetries, and polarization fractions in various charmless B decays at Belle II. We use a sample of electron-positron collisions at the $\Upsilon(4S)$ resonance from the SuperKEKB collider and corresponding to an integrated luminosity of 34.6 fb^{-1} in 2019 and 2020. All results are consistent with world average and provide extensive validations of the detector performances and analysis strategies.

The 19th International Conference on B-Physics at Frontier Machines (BEAUTY 2020)

21-24 September, 2020

Remote conference

^{*}Speaker.

[†]On behalf of the Belle II Collaboration.

1. Introduction

Charmless B decays are important to search for non-standard-model physics in the flavor sector. The decays via penguin amplitude are sensitive to non-Standard-Model (non-SM) contributions contributing to the loop. It is one of the most important target of the Belle II experiment. With larger amount of data, Belle II will significantly improve the associated physics measurements, such as determination of the CKM phase α/ϕ_2 [1, 2], examination of $K\pi$ isospin sum rule [1, 3], and CP asymmetry and intermediate resonance localized in phase space of three-body B decays [1]. The measurement of decay-time dependent CP violation in the penguin-dominated $B^0 \rightarrow \phi K^0$ mode, compared with corresponding results from $B^0 \rightarrow J/\psi K^0$ decays, offers a sharp probe of non-SM physics

We are also interested in the longitudinal polarization fraction (f_L) in the vector-vector $B \rightarrow \phi K^*$ decays. Previous measurements on f_L of $B^0 \rightarrow J/\psi K^0$ show a sizable contribution from transverse polarization, while the longitudinal polarization is predicted to be dominant. Although this effect can be understood nowadays [4, 5], the f_L measurement is still important to check the effects from non-uniform detector acceptance.

SuperKEKB [6] is an asymmetric e^+e^+ collider, and it started the collision operations with the Belle II detector [7] from March 2019. We use a skimmed good-quality data sample of 34.6 fb^{-1} , which was collected at the $\Upsilon(4S)$ resonance up to May 2020. This report will present the first reconstruction first measurements of branching fractions (\mathcal{B}), CP -violating charge-asymmetries (\mathcal{A}_{CP}) and longitudinal polarization fractions (f_L) based on 12 charmless B decays with Belle II data: $B^0 \rightarrow K^+\pi^-$, $B^0 \rightarrow \pi^+\pi^-$, $B^+ \rightarrow K^+\pi^0$, $B^+ \rightarrow \pi^+\pi^0$, $B^+ \rightarrow K^0\pi^+$, $B^0 \rightarrow K^0\pi^0$, $B^+ \rightarrow K^+K^-K^+$, $B^+ \rightarrow K^+\pi^-\pi^+$, $B^0 \rightarrow \phi K^0$, $B^+ \rightarrow \phi K^+$, $B^0 \rightarrow \phi K^{*0}$, and $B^{*+} \rightarrow \phi K^{*+}$ [8, 9].

2. B candidate reconstruction and event selection

The B reconstruction, event selection criteria, and background suppression scheme are studied with various Monte Carlo simulation samples for both signal decays and background. Charged-particle trajectories (tracks) are identified with inner vertex detectors and central drift chamber with requirements on the impact parameters to reduce beam-background-induced tracks. The identification of charged particles uses the information from two PID devices: time-of-propagation counter in barrel region and proximity focusing Aerogel ring image Cherenkov counter in forward endcap region. Decays of π^0 candidates are reconstructed by using two isolated clusters in the Electromagnetic Calorimeter, with requirements on the helicity angle and kinematic fit to constrain π^0 mass. Decays of K_S^0 candidates are reconstructed with two opposite-charged pion tracks from a common vertex, and restricted to meet additional requirements on its kinematic variables, e.g. momentum, flight distance, distance between pion trajectories, etc, to further reduce the combinatorial background. Decays of ϕ candidates are reconstructed with two opposite-charged kaon tracks. Decays of K^{*0} candidates are reconstructed with one K^+ and one π^- , and K^{*+} are reconstructed with one K_S^0 and one π^+ . In three body decays, we suppress the obvious peaking backgrounds from charmed or charmonium intermediate states by excluding the corresponding two-body mass ranges.

We use the following two major variables to distinguish the signal B events from other backgrounds: Energy difference between the reconstructed B candidate and half of the collision energy

in $\Upsilon(4S)$ frame ($\Delta E \equiv E_B - \sqrt{s}/2$), and Beam-energy-constrained mass ($M_{bc} \equiv \sqrt{s/(4c^2) - (p_B^*/c)^2}$).

3. Continuum background suppression

One of the main challenges of the charmless B decays' search is the large combinatorial background with the same final state from the $e^+e^- \rightarrow q\bar{q}$ ($q = u, d, s, c$) processes. It is mainly due to small branching fraction ($O(10^{-5})$) and the lack of final-state features (leptons or intermediate resonances), such that the reconstructed decay is hardly distinguished with continuum event. A binary boosted decision-tree (BDT) classifier is used to combine more than 30 variables nonlinearly. The input variables to BDT include event topology variables, flavor-tagging information, vertex-fitting information, and kinematic-fit information. All of them are required to be loosely or not correlated to ΔE and M_{bc} .

4. Signal extraction and measurement results

We use unbinned maximum likelihood fit to extract numbers of signal yield from the data sample to calculate various physics observables. In addition to ΔE and M_{bc} , there are five more variables involved in the fit: Output of the continuum suppression BDT discriminator (C'_{out}), K^+K^- candidate mass ($m_{K^+K^-}$), ϕ candidate's cosine of the helicity angle ($\cos\theta_{H,\phi}$), $K^+\pi^-$ candidate mass ($m_{K\pi}$), and K^* candidate's cosine of the helicity angle ($\cos\theta_{H,K^*}$). The $B \rightarrow hh$ and $B \rightarrow hhh$ ($h = K$ or π) modes use ΔE only with $M_{bc} > 5.27 \text{ GeV}/c^2$ in the data fit. The two $B \rightarrow \phi K$ modes use five variables excluding $m_{K\pi}$ and $\cos\theta_{H,K^*}$. The two $B \rightarrow \phi K^*$ modes use all the seven variables above.

After obtaining the signal yields by fitting on data, we determine:

- Branching fraction: $\mathcal{B} = \frac{N}{\varepsilon \times 2 \times N_{BB}}$, where N is the signal yield, ε is the signal reconstruction efficiency, and N_{BB} is the number of $B\bar{B}$ events (19.7M for B^+B^- and 18.7M for $B^0\bar{B}^0$). ε is obtained by using simulation and is validated with control samples. N_{BB} is obtained from the measured integrated luminosity, the exclusive $e^+e^- \rightarrow \Upsilon(4S)$ cross section, and $\mathcal{B}(\Upsilon(4S) \rightarrow B^0\bar{B}^0)$ [10].
- CP asymmetry: The raw asymmetry is obtained by $\mathcal{A} = \frac{N(b) - N(\bar{b})}{N(b) + N(\bar{b})}$, where $N(b)$ and $N(\bar{b})$ are the yields of the final state with b and \bar{b} flavors, respectively. The CP asymmetry is obtained by considering the instrumental effect: $\mathcal{A} = \mathcal{A}_{CP} + \mathcal{A}_{det}$. $\mathcal{A}_{det}(K^+\pi^-) = -0.010 \pm 0.003$ and $\mathcal{A}_{det}(K_S^0\pi^+) = -0.010 \pm 0.003$ are measured by using large samples of $D^0 \rightarrow K^+\pi^-$ and $D^+ \rightarrow K_S^0\pi^+$ decays with negligible CP violation. Then, $\mathcal{A}_{det}(K^+) = -0.015 \pm 0.022$ is obtained from $\mathcal{A}_{det}(K^+) = \mathcal{A}_{det}(K^+\pi^-) - \mathcal{A}_{det}(K_S^0\pi^+) + \mathcal{A}_{det}(K_S^0)$ [11].
- Longitudinal polarization fraction: $f_L = \frac{N_L/\varepsilon_L}{N_L/\varepsilon_L + N_T/\varepsilon_T}$, where $N_{L(T)}$ and $\varepsilon_{L(T)}$ is the signal yield and signal reconstruction efficiency with longitudinal (transverse) polarization, respectively. The distinctive helicity angle distributions allow for separating the two signal components (Figure 1).

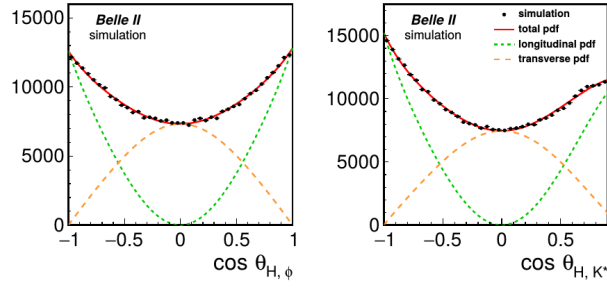


Figure 1: Distributions of $\cos\theta_{H,\phi}$ and $\cos\theta_{H,K^*}$ for simulated $B \rightarrow \phi K^*$ signal events. The green dashed (orange long dashed) lines are the PDFs of the longitudinal (transverse) components.

Figures 2–9 show the ΔE distributions in data for $B^0 \rightarrow K^+ \pi^-$, $B^0 \rightarrow \pi^+ \pi^-$, $B^+ \rightarrow K^+ \pi^0$, $B^+ \rightarrow \pi^+ \pi^0$, $B^+ \rightarrow K^0 \pi^+$, $B^0 \rightarrow K^0 \pi^0$, $B^+ \rightarrow K^+ K^- K^+$ and $B^+ \rightarrow K^+ \pi^- \pi^+$ decays, with fit projection overlaid. Figure 10 shows the ΔE , M_{bc} , C'_{out} , m_{K+K^-} , and $\cos\theta_{H,\phi}$ distributions in data for $B^+ \rightarrow \phi K^+$ and $B^0 \rightarrow \phi K^0$ decays, with fit projection overlaid. Figure 11 shows the ΔE , M_{bc} , C'_{out} , m_{K+K^-} , $\cos\theta_{H,\phi}$, $m_{K\pi}$, and $\cos\theta_{H,K^*}$ distributions in data for $B^+ \rightarrow \phi K^{*+}$ and $B^0 \rightarrow \phi K^{*0}$ decays, with fit projection overlaid. The major systematic uncertainties come from tracking, PID, and PDF modelling. All the measurement results are summarized in Table 1.

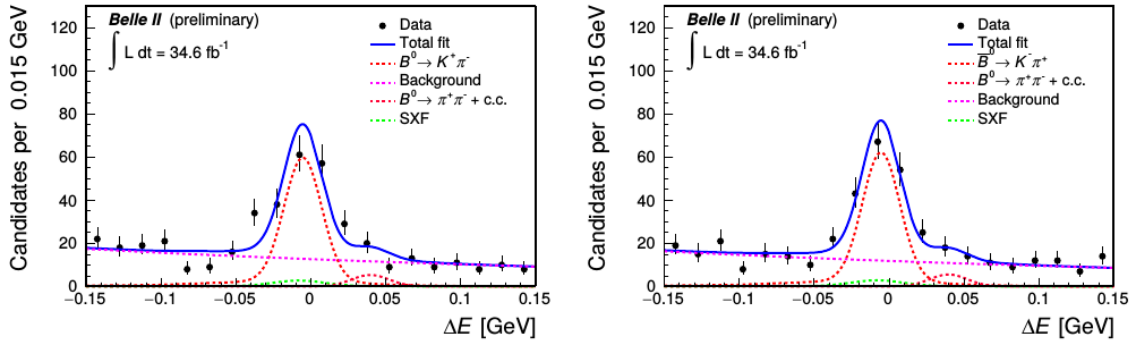


Figure 2: Distribution of ΔE for $B^0 \rightarrow K^+ \pi^-$ (left) and $B^0 \rightarrow K^- \pi^+$ (right) decays with fit projections overlaid.

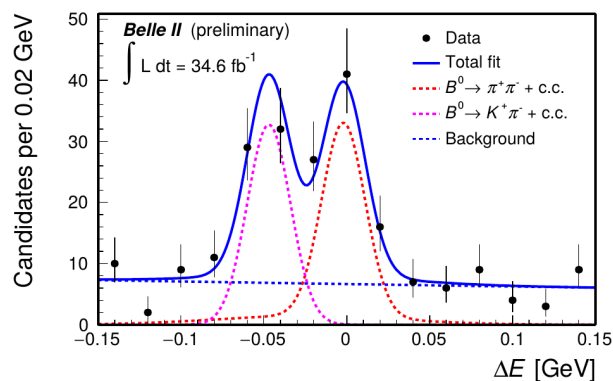


Figure 3: Distribution of ΔE for $B^0 \rightarrow \pi^+\pi^-$ decays with fit projections overlaid.

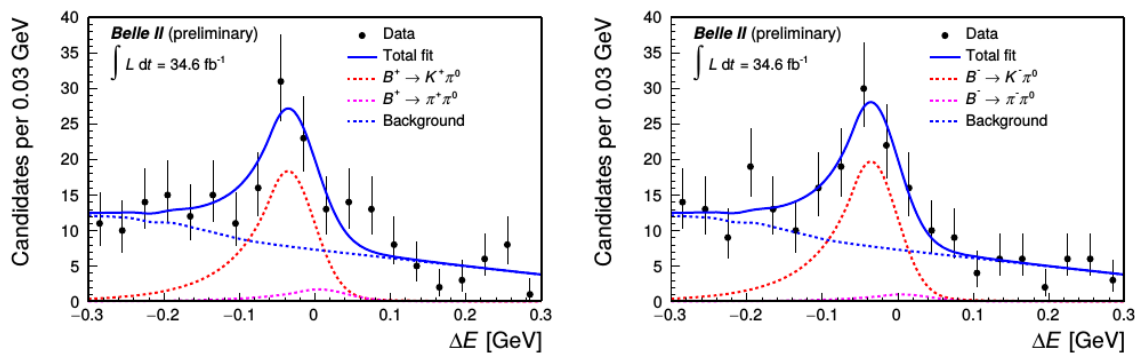


Figure 4: Distribution of ΔE for $B^+ \rightarrow K^+\pi^0$ (left) and $B^- \rightarrow K^-\pi^0$ (right) decays with fit projections overlaid.

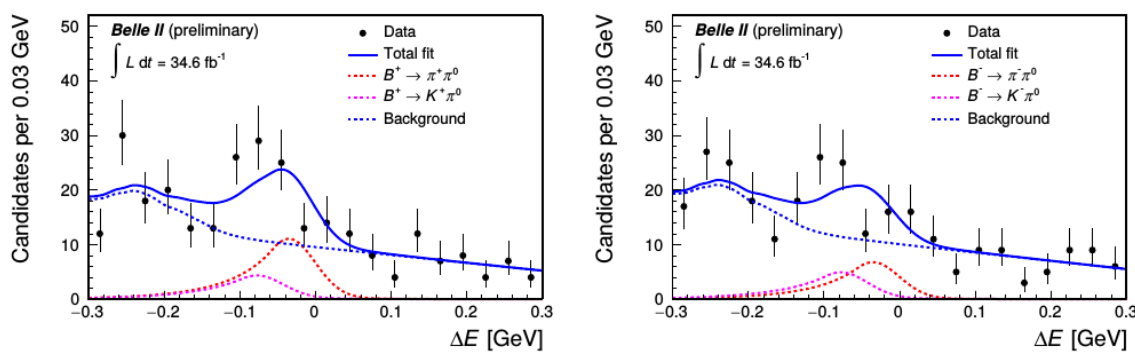


Figure 5: Distribution of ΔE for $B^+ \rightarrow \pi^+\pi^0$ (left) and $B^+ \rightarrow \pi^-\pi^0$ (right) decays with fit projections overlaid.

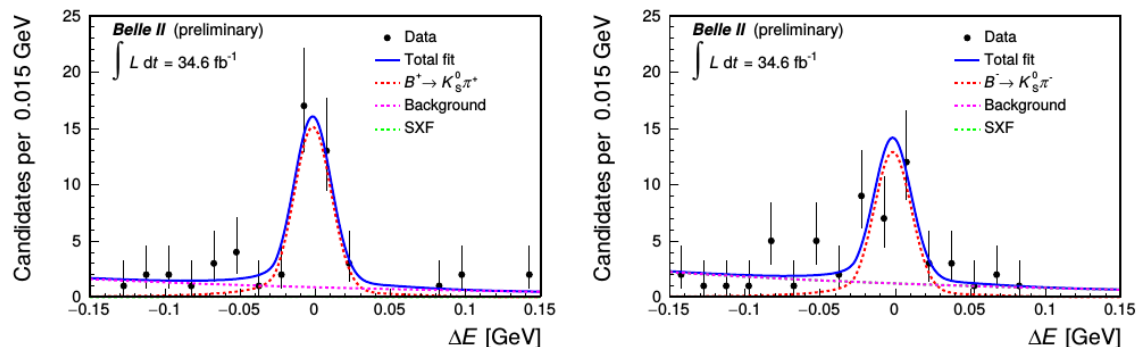


Figure 6: Distribution of ΔE for $B^+ \rightarrow K_S^0 \pi^+$ (left) and $B^- \rightarrow K_S^0 \pi^-$ (right) decays with fit projections overlaid.

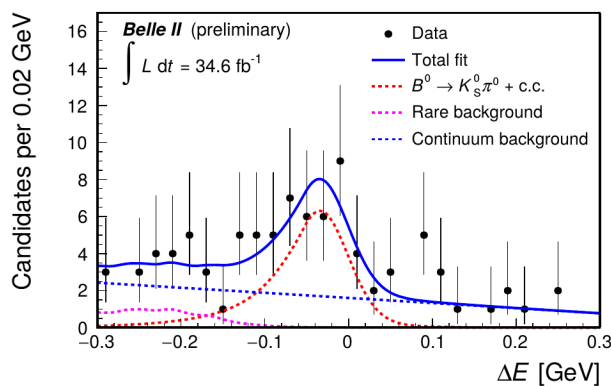


Figure 7: Distribution of ΔE for $B^0 \rightarrow K_S^0 \pi^0$ decays with fit projections overlaid.

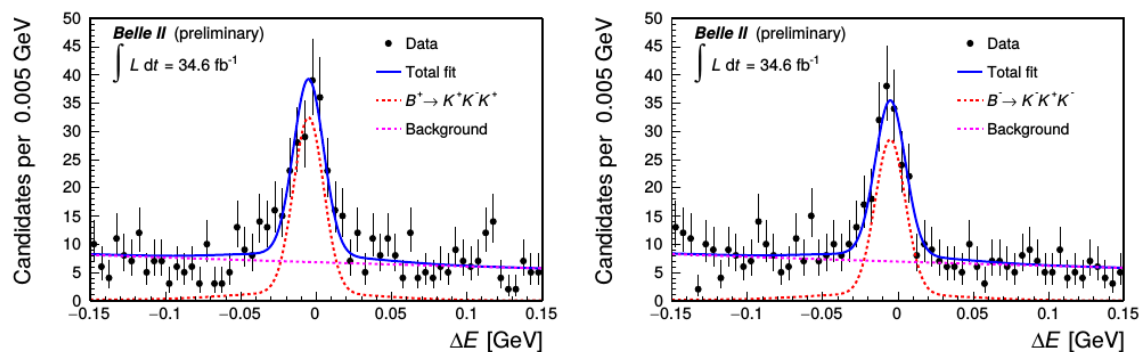


Figure 8: Distribution of ΔE for $B^+ \rightarrow K^+ K^- K^+$ (left) and $B^- \rightarrow K^- K^+ K^-$ (right) decays with fit projections overlaid.

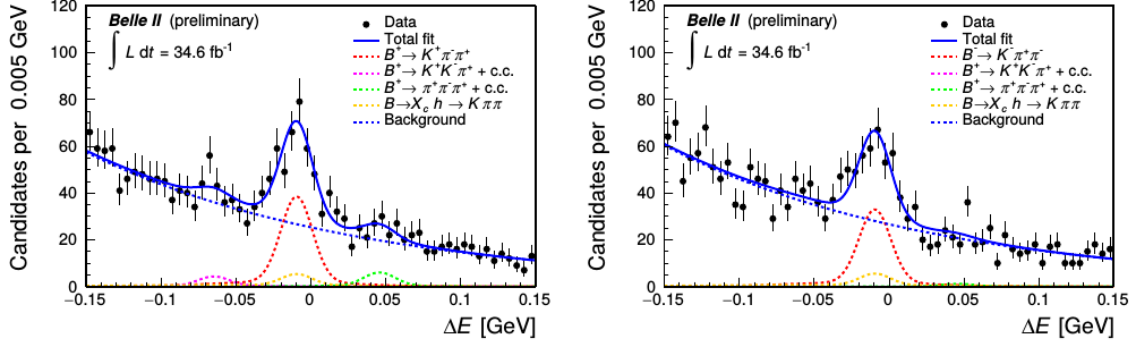


Figure 9: Distribution of ΔE for $B^+ \rightarrow K^+ \pi^- \pi^+$ (left) and $B^- \rightarrow K^- \pi^+ \pi^-$ (right) decays with fit projections overlaid.

Table 1: Summary of measurement results. The first errors in the values are statistical and the second ones are systematic.

Mode	\mathcal{B} (10^{-6})	\mathcal{A}_{CP}	f_L
$B^0 \rightarrow K^+ \pi^-$	$18.9 \pm 1.4 \pm 1.0$	$0.030 \pm 0.064 \pm 0.008$	-
$B^0 \rightarrow \pi^+ \pi^-$	$5.6^{+1.0}_{-0.9} \pm 0.3$	-	-
$B^+ \rightarrow K^+ \pi^0$	$12.7^{+2.2}_{-2.1} \pm 1.1$	$0.052^{+0.121}_{-0.119} \pm 0.022$	-
$B^+ \rightarrow \pi^+ \pi^0$	$5.7 \pm 2.3 \pm 0.5$	$-0.268^{+0.249}_{-0.322} \pm 0.123$	-
$B^0 \rightarrow K^0 \pi^+$	$21.8^{+3.3}_{-3.0} \pm 2.9$	$-0.072^{+0.109}_{-0.114} \pm 0.024$	-
$B^0 \rightarrow K^0 \pi^0$	$10.9^{+2.9}_{-2.6} \pm 1.6$	-	-
$B^+ \rightarrow K^+ K^- K^+$	$32.0 \pm 2.2 \pm 1.4$	$-0.049 \pm 0.063 \pm 0.022$	-
$B^+ \rightarrow K^+ \pi^- \pi^+$	$48.0 \pm 3.8 \pm 3.3$	$-0.063 \pm 0.081 \pm 0.023$	-
$B^0 \rightarrow \phi K^0$	$5.9 \pm 1.8 \pm 0.7$	-	-
$B^+ \rightarrow \phi K^+$	$6.7 \pm 1.1 \pm 0.5$	-	-
$B^0 \rightarrow \phi K^{*0}$	$11.0 \pm 2.1 \pm 1.1$	-	$0.57 \pm 0.20 \pm 0.04$
$B^{*+} \rightarrow \phi K^{*+}$	$21.7 \pm 4.6 \pm 1.9$	-	$0.58 \pm 0.23 \pm 0.02$

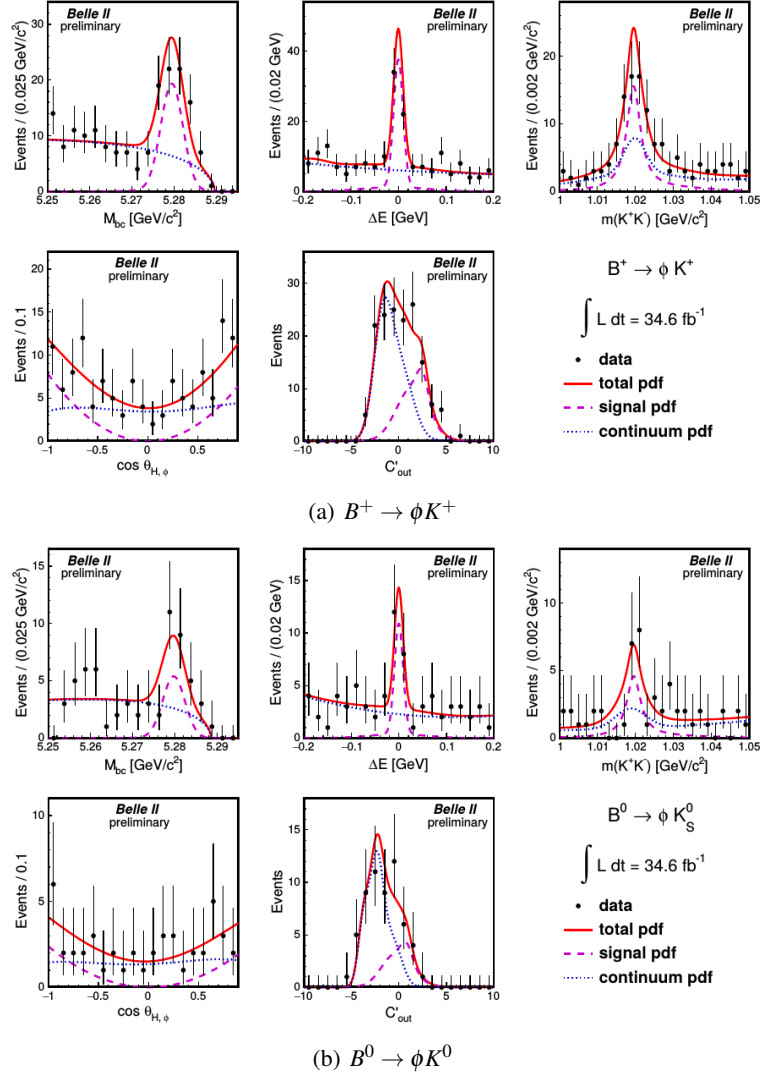


Figure 10: Distribution of ΔE , M_{bc} , C'_{out} , $m_{K^+K^-}$, and $\cos\theta_{H,\phi}$ for $B^+ \rightarrow \phi K^+$ and $B^0 \rightarrow \phi K^0$ decays with fit projections overlaid.

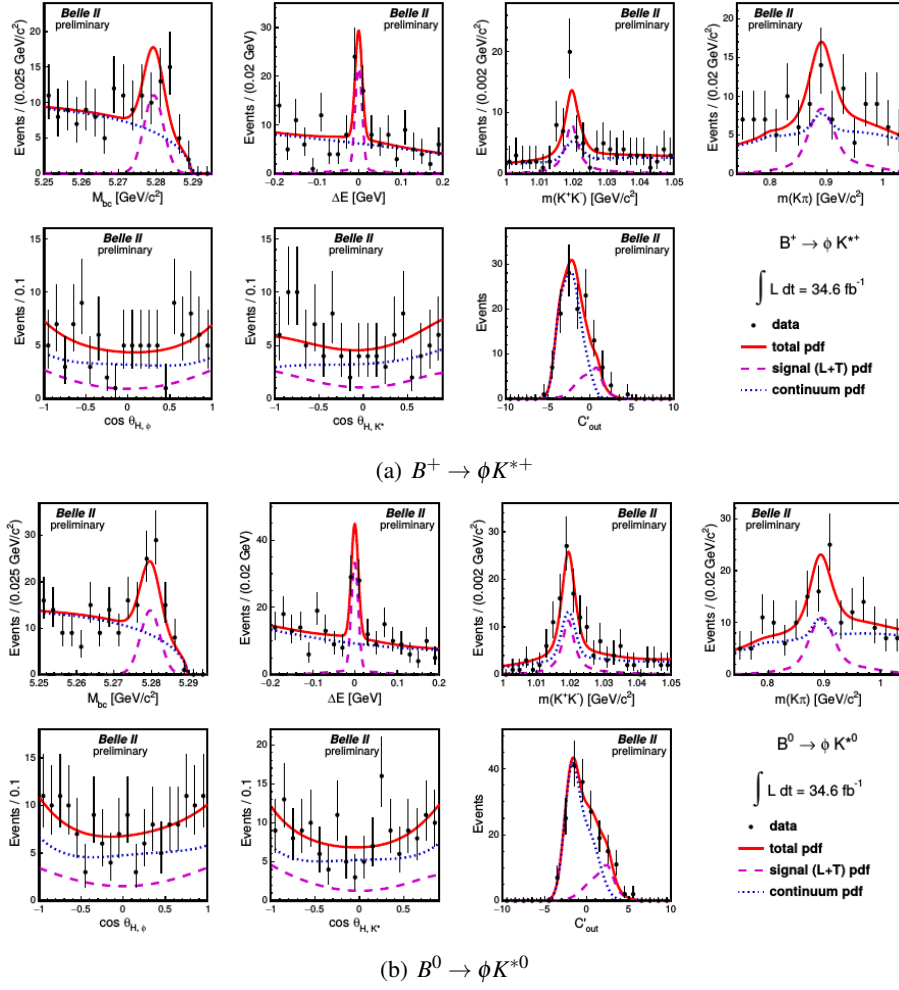


Figure 11: Distribution of ΔE , M_{bc} , C'_{out} , $m_{K^+K^-}$, $\cos\theta_{H,\phi}$, $m_{K\pi}$, and $\cos\theta_{H,K^*}$ for $B^+ \rightarrow \phi K^{*+}$ and $B^0 \rightarrow \phi K^{*0}$ decays with fit projections overlaid.

5. Summary

Belle II reports first measurements in charmless B decays with a data sample corresponding to 34.6 fb^{-1} . The measurements include branching fraction, CP asymmetry, and longitudinal polarization fraction of $B \rightarrow \phi K^*$ modes. All the results are in agreement with the known values, and offer good validations on the detector performance and analysis strategies.

References

- [1] E. Kou *et al.* (Belle II Collaboration), PTEP **2019** (2019) no.12, 123C01, arXiv:1808.10567 [hep-ex].
- [2] M. Gronau and D. London, Phys. Rev. Lett. **65** (1990) 3381 .
- [3] M. Gronau, Phys. Lett. B **627** (2005) no. 1, 82-88.
- [4] A. L. Kagan, Phys. Lett. B **601** (2004) no. 3 151-163.
- [5] M. Beneke, J. Rohrer, and D. Yang, Phys. Rev. Lett. **96** (2006) 141801.
- [6] K. Akai *et al.*, Nucl. Instrum. Meth. A **907** (2018) 188-199 .
- [7] T. Abe *et al.* (Belle II Collaboration), arXiv:1011.0352 [hep-ex].
- [8] F. Abudinén (Belle II Collaboration), arXiv:2009.09452 [hep-ex].
- [9] F. Abudinén (Belle II Collaboration), arXiv:2008.03873 [hep-ex].
- [10] A. J. Bevan *et al.* (Belle and BaBar Collaborations), Eur. Phys. J. **C74** (2014) 3026, arXiv:1406.6311 [hep-ex].
- [11] A. Davis *et al.* (LHCb Collaboration), [LHCb-PUB-2018-004].